Supplementary Information (SI) for RSC Medicinal Chemistry.
This journal is © The Royal Society of Chemistry 2024

Exploring 7β-Amino-6-Nitrocholestens as COVID-19 Antivirals: In silico, Synthesis, Evaluation, and Integration of Artificial Intelligence (AI) in Drug Design: Assessing the Cytotoxicity and Antioxidant Activity of 3β-Acetoxynitrocholestane

Table S1. Molecular docking analysis that examined the binding energies and hydrogen bond interactions of ligands with active-site amino acid residues of PLpro, 3CLpro/Mpro, and RdRp targets.

Compds	Receptors (PDB No#)	Binding Affinity (kcal/mol)	Intermolecular Interactions	
			Interacting Amino Acid Residues	Conventional Hydrogen Bonds
1	6lu7	-5.1	MET165, GLU166, GLN189, ASN142, MET49, GLY143, CYS145	1
	6m71	-7.2	LEU172, ARG249, PRO169, ASP170, LEU460, PRO461, PRO677, ASN459, ARG349, PHE396, CYS395, ARG457, THR394	1
	6w9c	-6.8	LYS306, THR259, GLY256, SER278, PHE258, LYS279, THR257, TYR305, HIS255, LYS217, TYR213, GLU214, GLU307	1
2	6lu7	6.1	ASN142, GLN189, GLU166, MET165, HIS163, CYS145, GLY143	1
	6m71	-7.0	ARG349, PHE396, CYS395, LEU172, THR394, ARG457, ARG249, LEU460, ASP170, ASN459, PRO461, PRO461, PRO677	1
	6w9c	-6.0	SER278, HIS255, GLY256, GLU124, GLN121, GLN122, LYS306, PHE258, THR259, LYS279	0
3	6lu7	-6.5	LEU167, THR190, Pro168, ALA191, GLN192, GLU166, HIS163, ASN142, LEU141, CYS145, GLY143, SER144, HIS164, HIS41, MET165, MET49, GLN189	2
	6m71	-7.6	PRO461, THR319, LEU251, THR246, ARG249, LEU460, VAL675, ARG349, PHE396, PRO677, THR394, CYS395, TYR456, ARG457, ASN459	1

	6w9c	-6.1	CYS155, ASN156, ARG82, PHE79, ASP76, THR74, TYR154, TYR171, GLN174, HIS175	2
4	6lu7	6.1	PRO168, THR190, GLN189, HIS41, MET49, GLY143, CYS145, MET165, ASN142, GLU166, HIS163, GLU166	0
	6m71	-7.4	ASP865, SER861, PHE594, ILE864, LYS593, GLN815, TRP598, MET601, CYS813, LEU758, GLY590, ILE589, VAL588, THR591, SER592	2
	6w9c	-6.2	THR257, TYR310, THR313, THR312, LYS217, LYS218, TYR213, TYR305, THR257, GLU307	1
5	6lu7	-6.4	MET165, GLU166, GLN189, SER46, MET49, THR25, THR26, GLY143, HIS41, ASN142,CYS145, SER144, LEU141	1
	6m71	-6.6	THR394, PHE396, PRO461, THR319, ARG349, PRO323, PHE321, TYR265, SER255	0
	6w9c	-6.1	GLU307, LYS306, THR259, SER278, GLY256, LYS279, PHE258, HIS255, TYR305, THR257, TYR213, LYS217	0
6	6lu7	-6.6	MET165, GLU166, GLN189, MET49, THR25, THR26, GLY143, HIS41, ASN142,CYS145, SER144, LEU141	0
	6m71	-7.0	LEU460, ASN459, PRO461, PRO677, ARG349, PHE396, CYS395, TYR456, THR394, LEU172, PRO323, PRO169, ARG457	0
	6w9c	-6.5	THR257, TYR305, GLU307, THR312, THR311, THR313, LYS217, LYS218, TYR213, TYR310, GLU214	1
7	6lu7	-5.8	MET49, HIS41, GLY143, CYS145, MET165, HIS164, ASN142, HIS163, GLU166, PRO168, THR190, GLN189	0
	6m71	-6.9	PRO461, ASN459, PRO677,	1

			ARG457, LEU172, PRO169, ARG249, THR394, PHE396, PRO323, ARG349, VAL675	
	6w9c	-6.5	GLY256, LYS306, THR257, GLU214, SER212, PHE258, TYR305, LYS254, LEU253, TYR251, GLU252	0
8	6lu7	-6.2	THR190, ALA191, GLN192, PRO168, GLU166, HIS163, ASN142, MET165, HIS164, HIS41, MET49, GLN189, CYS145, GLY143	2
	6m71	-7.0	PRO677, TYR456,ARG457, ASN459, CYS395, THR394, PHE396, PRO323, ARG349, THR319, THR246, ARG249, PRO461	2
	6w9c	-5.9	TYR137, ARG138, GLN133, PRO130, GLU70, ASP12, ILE14, ASN15, TYR71, ARG138	0
9	6lu7	-7.0	PHE140, LEU141, HIS163, ASN142, LEU27, GLY143, THR24, HIS41, THR25, THR26, CYS145, MET49, GLN189, GLU166	2
	6m71	-7.4	SER397, TYR149, PHE396, TYR265, LEU122, THR324, LYS267, TRP268, ILE266, PRO322, PHE321, VAL320, SER255	2
	6w9c	-7.2	LYS306, THR259, GLY256, THR257, GLU214, PHE258, TYR251, TYR305, LYS254, GLY256	0

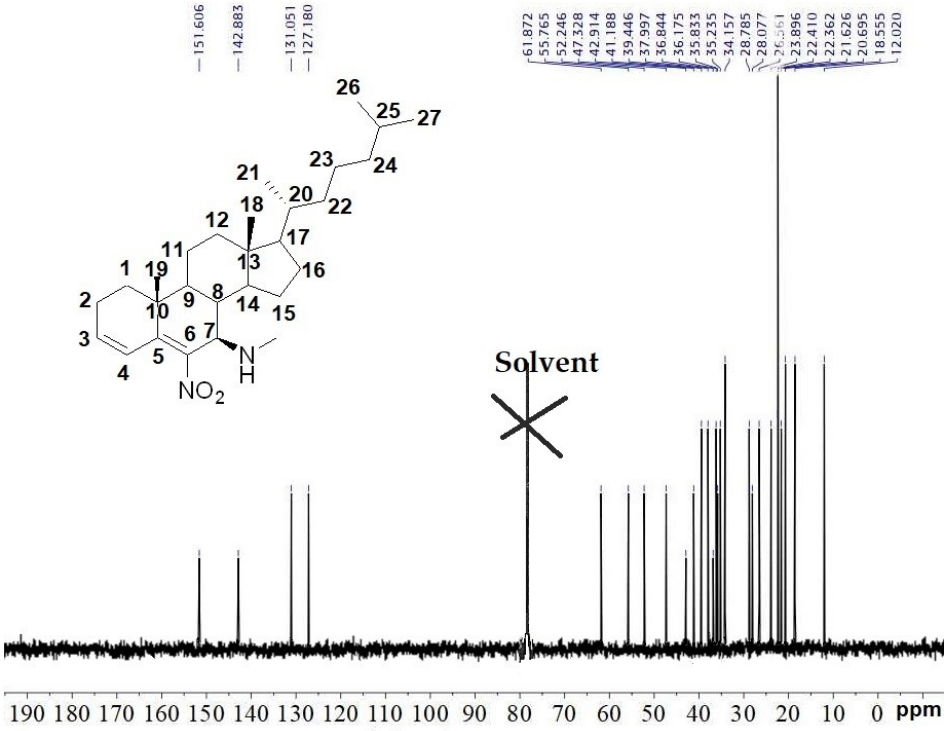

Figure S1. ^{13}C NMR spectrum of steroidal compound 4

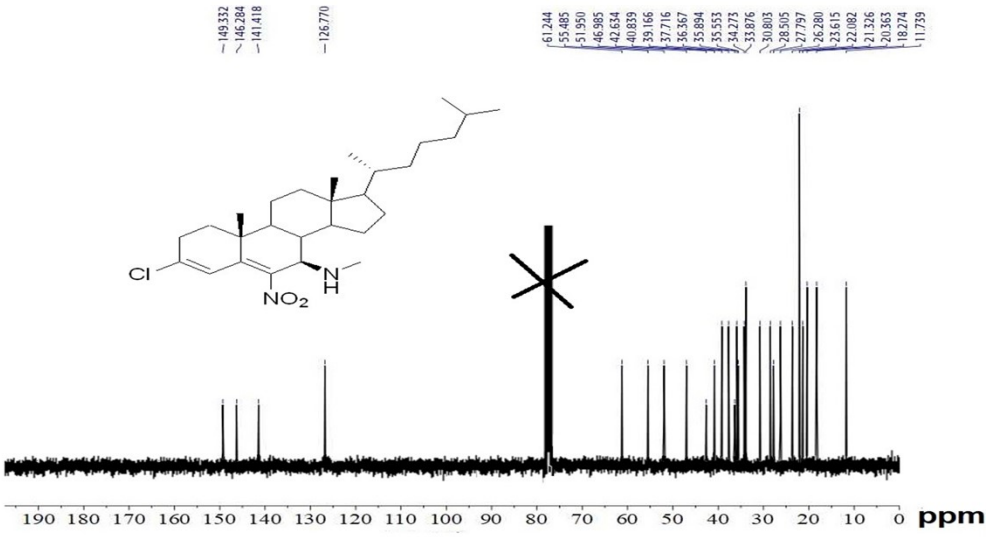

Figure S2. ^{13}C NMR spectrum of steroidal compound 5

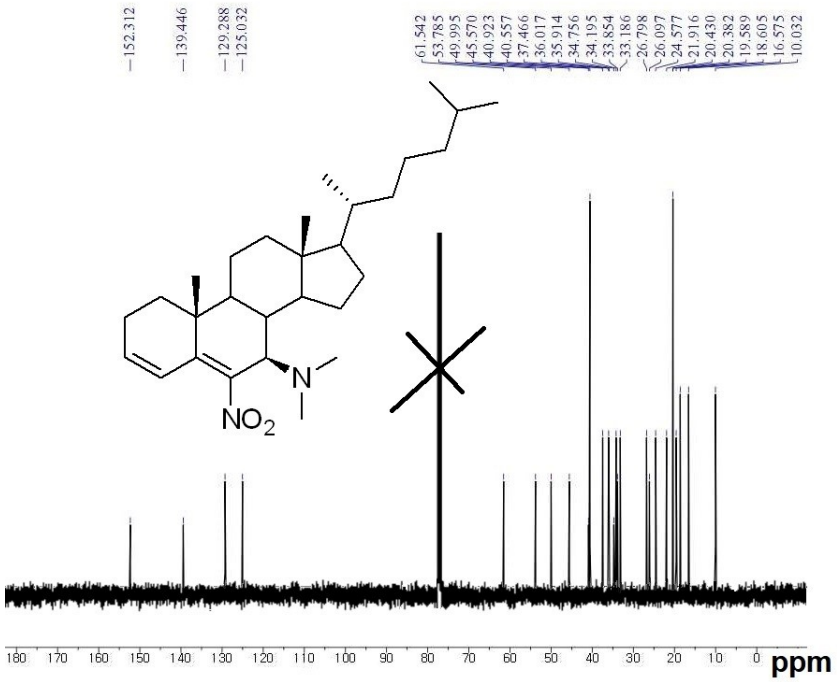

Figure S3. ^{13}C NMR spectrum of steroidal compound 6

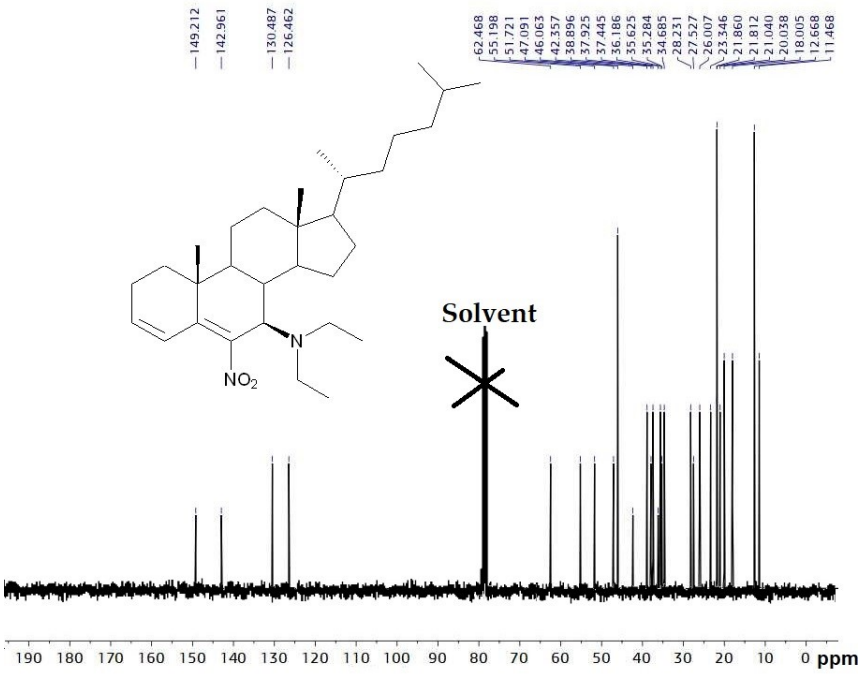

Figure S4. ^{13}C NMR spectrum of steroidal compound 7

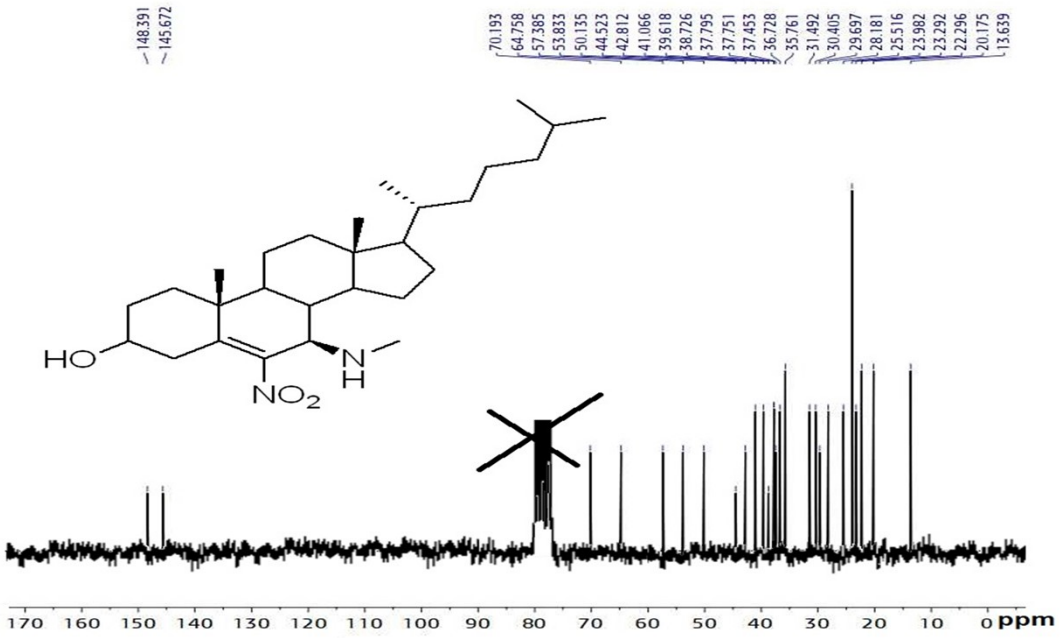

Figure S5. ^{13}C NMR spectrum of steroidal compound 8

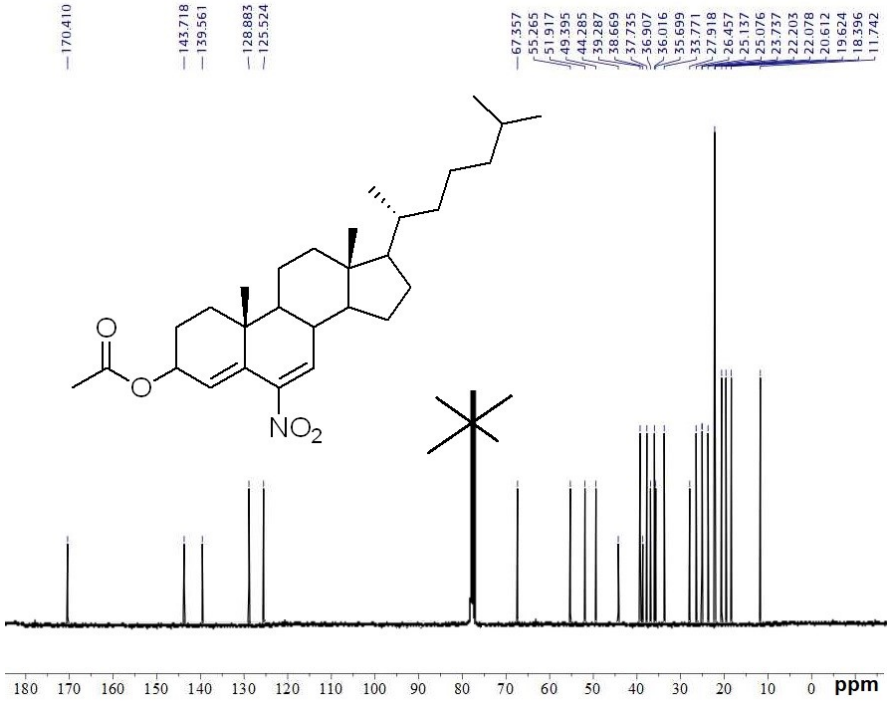

Figure S6. ^{13}C NMR spectrum of steroidal compound 8

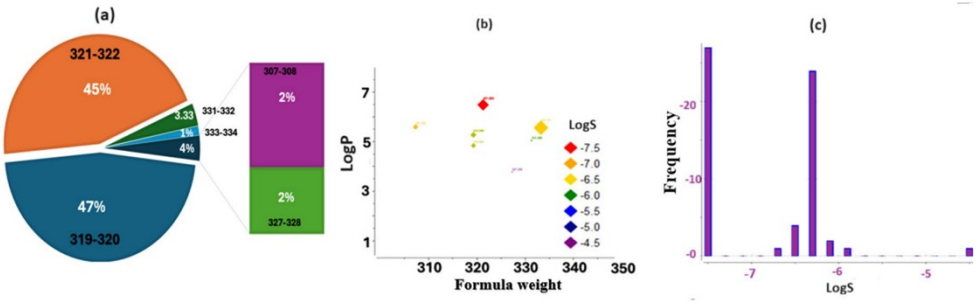

Figure S7 displays descriptors for 60 AI-generated molecules. (a) Shows the AI molecules with their division in molecular weight percentages. (b) and (c) plot molecular weight (Weight) against molecular lipophilicity (LogP) and solubility (LogS).

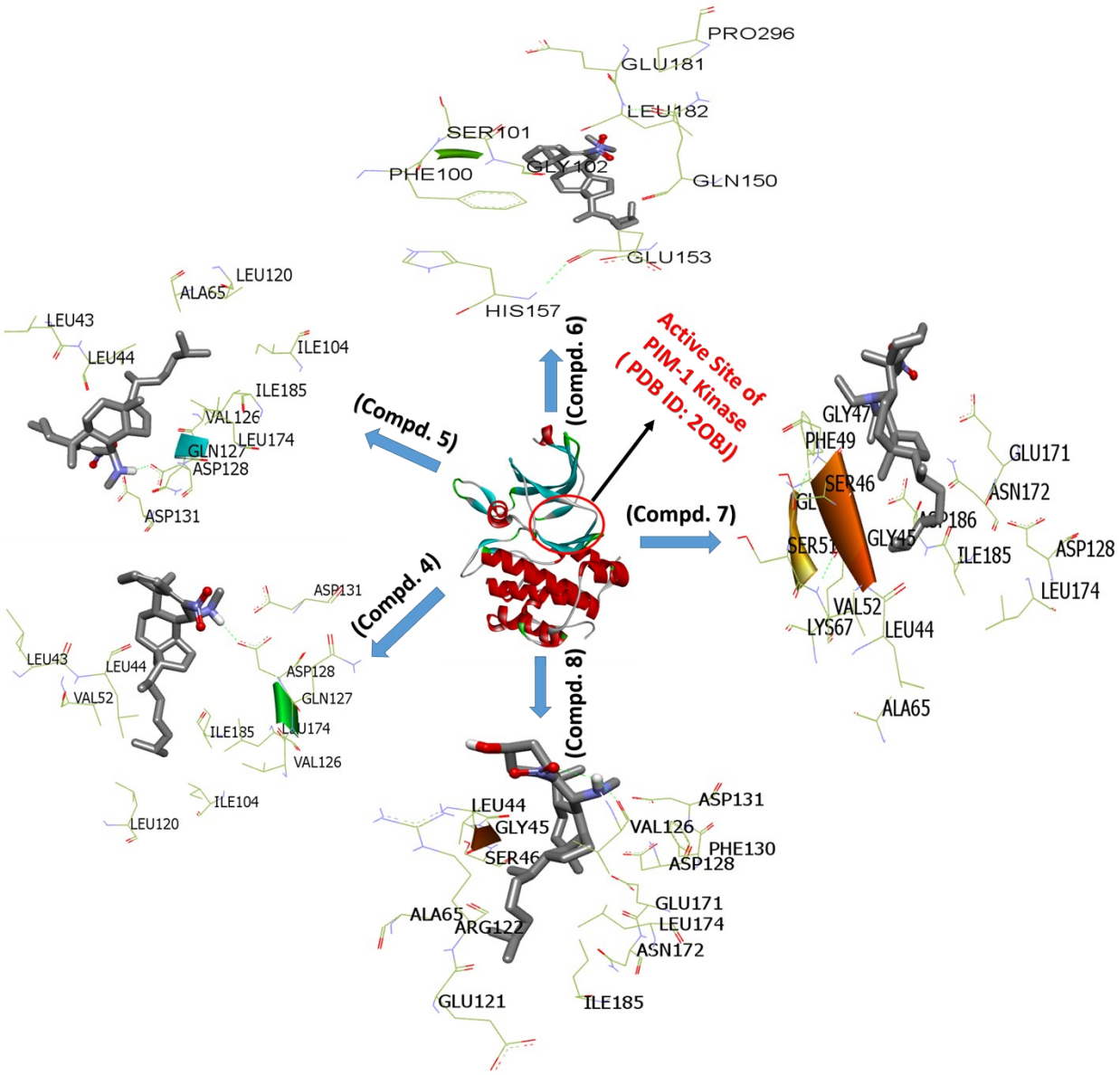

Figure S8. Nonbonding Interactions of Compounds 4-8 with Human PIM-1 Kinase (PDB: 2OBJ) from Molecular Docking

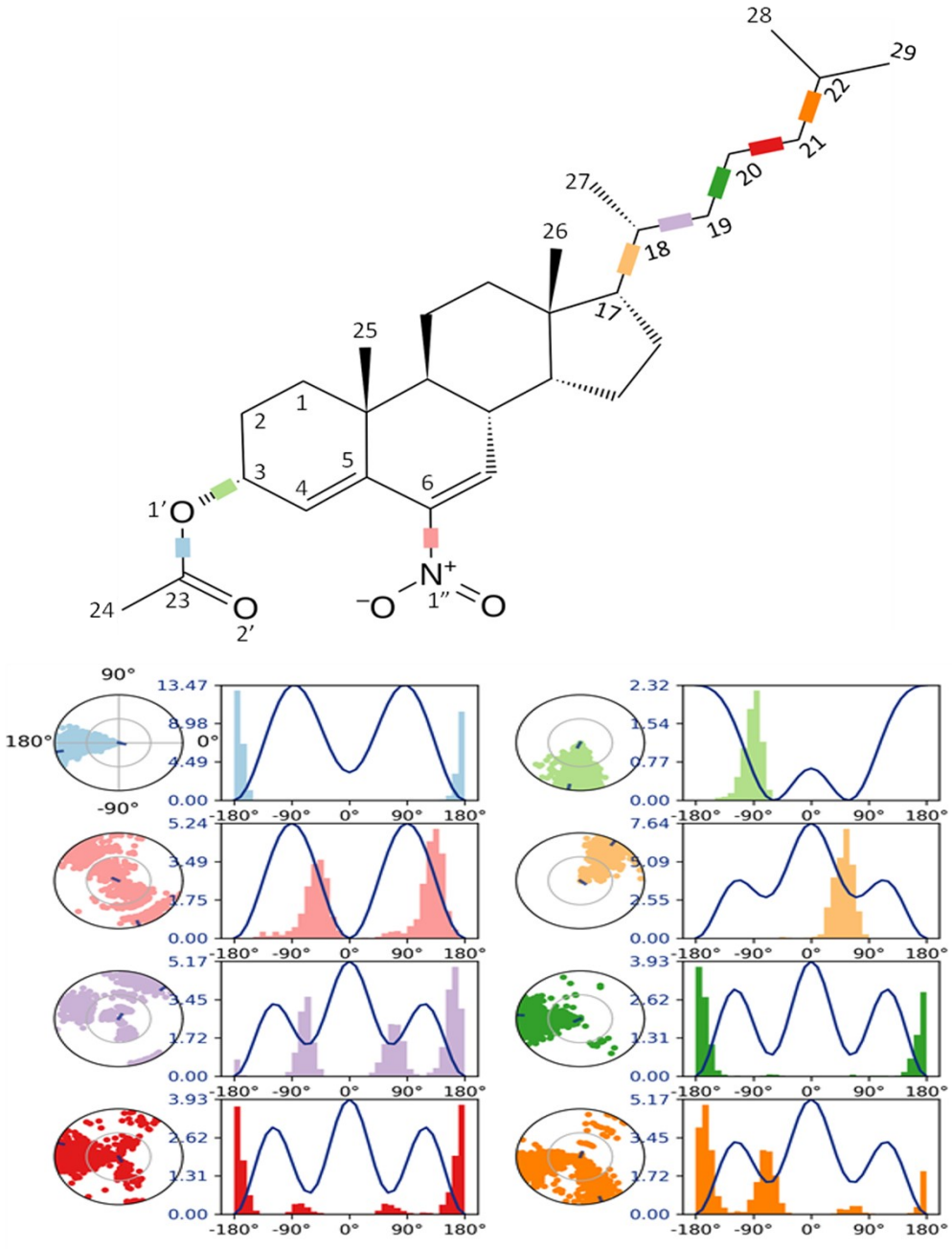

Figure S9. During the simulation, the ligand torsion profile of Compound-1 depicts the distribution of scaffold dihedrals. The conformational development of each rotatable bond (RB) in the ligand throughout the course of the simulation trajectory (0.00 to 100.00 ns) summarized in the ligand torsions graphic. The 2d dimensional graphic of a ligand with color-coded rotatable bonds is displayed in the top panel. A dial plot and matching coloured bar plots are included for each rotatable bond torsion. Dial (or radial) charts depict the confirmation of the torsion during the simulation. The beginning of the simulation is in the center of the radial plot and the time evolution is plotted radially outwards.

The torsion angle profile in the MD simulation is produced partially by the flexible side chain of the ligand (9) skeleton (Figure S9). The simulation starts with the various conformations that are radially outward recorded for each rotatable bond. Bar plots show the probability density of each torsional rotation. The contact between a ligand and a receptor, which resides in a rigid structure that can sustain the same binding orientation throughout the simulation, produces a smaller band with less diversity. The ligand torsion profile analysis offers useful information for identifying the pharmacophore features required for interacting with important residues in proteins. In Figure 2, the eight rotatable bonds (RB) of the ligand—C3-O1', O1'-C23, C6-N1", C17-C18, C18-C19, C19-C20, C20-C21, and C21-C22—that are represented by the colours green, blue, pastel red, yellow, violet, dark green, red, and orange show the ligand's strong conformational flexibility. The ratable bonds (RB) at the start of the simulation (0°) O3'-C23 and C17-C18 RBs are affected by the rigid ligand rings and methyls C25 and C26, which have high potential energies of 13.47 and 7.64 kcal/mol, respectively. Additionally, the MD simulation showed that the ligand's stiff core remained stable in complexes. The nitro group nitrogen atom and the oxygen atom -C-O-C-are involved in a binding contact, while the other oxygen atom is involved in a non-binding interaction. This suggests that the oxygen atom of the ligand ring was successful in firmly attaching protein. An illustration of the ligand's characteristics solely determined by the oxygen atom may be seen in Figure S9.